Anomalous phases in cavity-free 240 GHz Pulsed ENDOR spectra of 1.44 GeV Xe-irradiated LiF

J. van Tol
Center for Interdisciplinary Magnetic Resonance, National High Magnetic Field Laboratory, Florida State University, 1800 E. Paul Dirac Drive, Tallahassee, FL 32310 - 3706, USA

K.-P. Dinse*
Fachbereich Physik, Freie Universität Berlin, Arnimallee 14, 14195 Berlin, Germany

H. Stork
Institut für Festkörperphysik, TU Darmstadt, Hochschulstrasse 6, 64289 Darmstadt, Germany; present address: Laboratoire National des Champs Magnétiques Intenses, 143 avenue de Rangueil, 31400 Toulouse, France

F. Fujara
Institut für Festkörperphysik, TU Darmstadt, Hochschulstrasse 6, 64289 Darmstadt, Germany

B. Schuster, K. Schwartz
GSI-Helmholtzzentrum für Schwerionenforschung GmbH, 64291 Darmstadt, Germany
(Dated: July 9, 2012)

Paramagnetic centers generated by swift heavy ion irradiation of LiF crystals could be identified as electrons trapped at regular anion vacancy sites (F centers). Well resolved ENDOR spectra resulting from hfi with ^{7}Li and ^{19}F nuclei located in six different shells could be recorded. In order to preserve the mm-sized crystals, a cavity-free set up was used for the ENDOR experiments at an electronic Larmor frequency of 240 GHz. Apparently even under conditions of extremely high local energy loss in the ion track, the local density of persistent F centers is still sufficiently low to prevent distortions of the ionic crystal. The spread of hyperfine coupling constants was less than 5%. Neither in EPR nor in ENDOR spectra there was evidence for different types of paramagnetic centers. When performing ENDOR by applying the rf pulse directly after the 3-pulse Mims-type mw sequence, an anomalous ENDOR effect was observed. The observed "positive" and "negative" ENDOR response can be attributed to efficient hole and anti-hole formation in the inhomogeneously broadened EPR spectrum and can be used to determine the sign of hyperfine coupling constants.

I. INTRODUCTION

In a previous contribution we described the effect of point defects on the nuclear spin relaxation rates, which have been generated in a series of LiF crystals by Xe ion irradiation with swift heavy ions of MeV to GeV kinetic energy with varying fluences[1]. In a related study, the defects were were also investigated by optical spectroscopy[2]. The energy loss of such ions along the trajectory can reach up to several tens of keV per nanometer thus forming defects with very high density. A large variety of charged and uncharged defects was detected. For further characterization a high frequency EPR study was initiated, taking advantage of the improved spectral resolution at such high Larmor frequencies. To our surprise we noticed that even for samples exposed to high ion fluences the spin relaxation rates of the paramagnetic centers were quite moderate, thus allowing us to perform pulsed EPR at 240 GHz. We anticipated that these rather small relaxation rates would allow us to perform ENDOR experiments as well, thus providing detailed information about the nature of the EPR active centers. We focused on the identification of these paramagnetic centers, apparently acting as strong relaxation sinks for the nuclear spins. From partially resolved hyperfine interaction (hfi)in the EPR spectra there was already evidence that also in our case centers originate from electrons trapped on anion vacancy sites (F-centers). These specific paramagnetic centers had previously been generated by exposing to X-rays[3] or by neutron irradiation of a large variety of ionic crystals, and have been studied in great detail many decades ago[4]. Using ENDOR we expected to be able to confirm that F centers are the dominant species even under intense swift ion irradiation. Furthermore it should be possible to confirm or exclude the presence of different additional centers which might be hidden under the broad unresolved EPR line.

In the course of our investigation we noticed that ENDOR signals measured at liquid helium temperatures appeared in abnormal phases, i.e., ENDOR lines in a given experimental spectrum appeared as well in "absorption" as in "emission". Such effects were observed previously by different groups and have been used to determine the sign of the corresponding hfi[5–10]. Pioneering contributions of the groups of J. Schmidt (Leiden)[5] and D. Goldfarb (Rehovot)[6] have identified the relevant parameters

for specific pulse sequences and excitation conditions, which could lead to noticeable deviations from line intensities in "Boltzmann-equilibrated" ENDOR spectra. Later work of Stoll et al.[8] and Morton et al.[9] gave a quantitative description of effects to be expected, when using a Davies mw/rf pulse sequence with a different relative timing of mw and rf pulses. It was pointed out that the anomalous phase of ENDOR lines could be used for the determination of the sign of hyperfine coupling constants.

The determination of the sign of spin Hamilton parameters like fine structure (FS) or hyperfine interaction (hfi) is an important step in the final identification of paramagnetic centers. If for instance large FS terms in high-spin systems are present, the sign of the principal component can be readily obtained by determining the population of spin levels in thermal equilibrium at sufficiently low temperatures via relative EPR line intensities. This simple "Boltzmann equilibrium" method is also applicable to determine the sign of hfi constants via ENDOR experiment, if the sign of the g factor of the nuclear spin is known. The intensities of ENDOR transitions are proportional to the population differences within a given electron spin m_S manifold, which in turn are depending on the total population of this particular m_S level. The combination of electronic Larmor frequencies $\geq$ 200 GHz and liquid helium temperatures leads to a nearly complete depletion of higher electron spin levels, thus preventing detection of the complete set of ENDOR transitions originating from all m_S manifolds. Because of missing ENDOR lines, the analysis of crowded spectra and in particular the identification of participating nuclei can be impeded.[11]

In pulsed ENDOR, taking advantage of the rather long electron spin relaxation rates, it is possible to significantly populate the upper m_S manifold of a S = 1/2 center either by an initial inverting π-pulse (Davies sequence), or by a two-pulse echo sequence (Mims sequence). In both of these standard pulsed ENDOR methods, the rf pulse is applied after the preparation steps, its effect on the level populations being probed by a final Hahn echo sequence, or a single $\pi/2$-pulse, respectively. Depending on the relative timing of pulses, the sequence repetition rate, and the electronic spin relaxation rates, a complicated situation arises with respect to the relative intensity of lines belonging to different m_S ENDOR subsets.

Quite frequently, only a small fraction of the inhomogeneously broadened EPR line is probed by the train of (frequency-selective) microwave pulses. The final response (a Hahn or a stimulated echo) is a measure of the population difference of the selected spin packets. Repetitive excitation of a small part of the spin system even without the action of resonant rf transitions can lead to a significant change of its average spin temperature, even without changing the total number of spins (spin packet population) contributing to the excited transition. More important is the possibility that the combined action of mw and rf transitions leads to a redistribution of spin packet populations within the inhomogeneously broadened EPR line, which can be described as hole and anti-hole burning. The only relevant parameter for restoring the equilibrium Gaussian distribution of spin packet populations then is the nuclear spin relaxation time, which is usually much longer than electronic relaxation times and the pulse repetition time. (Here we assume that spectral shifts related to holes or anti-holes are too large to be covered even by multi-step spectral diffusion, a condition quite generally met in high frequency ENDOR.)

Using this model of combined mw/rf induced population transfer, a quite simple scenario emerges, allowing for a qualitative prediction of relative ENDOR line intensities without calculating in detail the effect of a repetitive multi-pulse sequence necessitating the knowledge of a large set of parameters. For our system the validity of this qualitative prediction was experimentally verified by using a modified Mims sequence, in which the rf pulse is applied directly after the stimulated echo. The scenario is similar to the modified Davies sequence suggested by Morton et al.[9], by which also the relative intensity of ENDOR lines was affected by modifying the relative timing of the rf pulse.

II. EXPERIMENTAL

Pulsed ENDOR experiments have been performed at the National High Magnetic Field Laboratory (NHMFL) in Tallahassee (USA). In order to preserve the crystal, a cavity-free setup was chosen for the investigation of samples of typical size 3x2x2 mm^3. Crystals were mounted in front of a mw mirror[12], the rf field being generated by a 4 turn coil wrapped around the sample. The "standard" 240 GHz pulsed EPR spectrometer operating in quasi optic mode was only slightly modified by increasing the mw field at the sample with a corrugated wave guide with an exit diameter of only 2 mm. The mw $\pi/2$ pulse length obtained with a source power of 40 mW was approximately 350 ns. Transitions within the nuclear spin levels were excited with an rf synthesizer, amplified to a level of 100 W. The output of the amplifier was terminated by the 50 Ω coaxial cable, terminated by the grounded 4 turn coil. No attempt was made to determine the local rf field amplitude.

Samples studied consisted of LiF crystals, being irradiated with swift (1.44 GeV) ^{130}Xe ions. Samples being exposed to different ion fluences were investigated. The samples were mounted with the (100) face of the face centered cubic crystal ($Fm\bar{3}m$) perpendicular to the external magnetic field B_0. Swift heavy ion bombardment leads to an inhomogeneous distribution of paramagnetic centers, resulting from the well defined stopping properties of the ion. The calculated insertion depth[13] was 87 μm in our case, consistent with results from spatially resolved NMR[1].

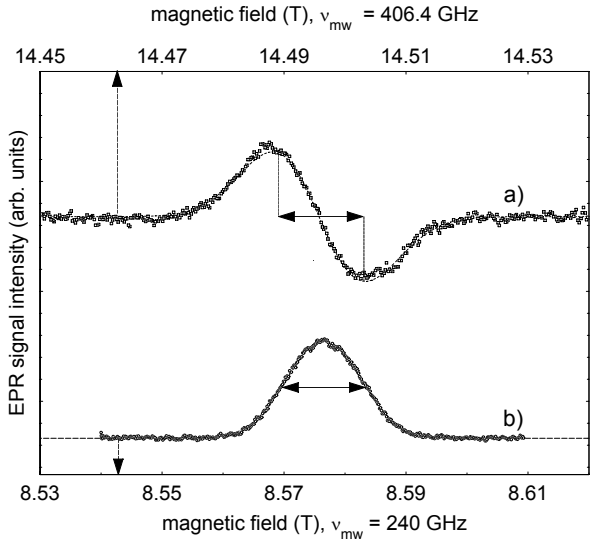

FIG. 1: Comparison of 240 GHz ESE (b) and 406 GHz c. w. EPR spectra (a) of Xe irradiated LiF. Both signals are fitted with a Gaussian line shape function. The FWHM of 14.3 mT and the peak-to-peak width of 15.2 mT are indicated by arrows. Spectra were taken at room temperature. Spectral display is performed by shifting the 406 GHz spectrum, but using the same field scale. The mw pulse sequence used for echo detection was 300-1000-360 ns, the field modulation amplitude used for c. w. EPR was 1 mT.

III. RESULTS AND DISCUSSION

A. EPR spectra

Preliminary pulsed EPR experiments revealed that even at room temperature the T_2 relaxation time was about 3 μs. Even with our rather restricted mw field resulting in typical mw pulse lengths of 350 ns, it was therefore possible to record electron spin echo (ESE) detected EPR spectra. In the lower trace of Fig. 1, the 240 GHz ESE spectrum of a LiF crystal irradiated with an ion fluence of $3 \cdot 10^{11}$ ions/cm^2 is shown. By comparing with a $Mn(II)$ standard, the total number of spins was estimated as $2 \cdot 10^{16}$. This value compares well with the area density of $6 \cdot 10^{16}$ cm^{-2}, determined optically. When comparing the excitation width with the total width of the EPR absorption, we conclude that the echo at the peak of the spectrum originates from approximately $8 \cdot 10^{13}$ spins. This value in turn can be used to estimate the minimum number of spins being detectable under optimal conditions in a fully Boltzmann polarized spin system at 5 K. Assuming a "polarization gain" of 42 and a room temperature signal-to-noise factor of at least 40, this number is estimated as $5 \cdot 10^{10}$ spins. This value compares well with numbers quoted for cavity-based spectrometers, reaching 10^7 as limiting number using a high Q resonator.

The spectrum can be fitted with a Gaussian line shape function. The Gaussian line shape is consistent with the assumption of inhomogeneous broadening by unresolved hfi with local Li and F spins. The observed line width of 14.3 mT (FWHM) corresponds to a variance $\sigma = 6.1$ mT of the Gaussian distribution function. This value is characteristic for V_F centers (trapped electron on a regular anion vacancy site). The close agreement with the line width measured at 9 GHz[1,3] and the absence of line asymmetry indicates that g matrix anisotropy is negligible. The high quality of the fit of the spectrum obtained at 240 GHz further indicates that no additional paramagnetic centers with deviating g values are detected in this ESE experiment. This observation is further supported by comparing spectra taken at an even higher Larmor frequency. In the upper trace of Fig. 1 the 406 GHz c. w. EPR spectrum is shown together with the 240 GHz ESE spectrum. The c. w. spectrum can also be simulated with a Gaussian shape function, the small increase in width ($\sigma = 7.6$ mT) being partially caused by broadening using field modulation with 1 mT field amplitude. Again no spectral features of additional paramagnetic centers are detected.

The temperature dependencies of spin dephasing and saturation recovery times are depicted in Figs. 2 and 3 for the "$3 \cdot 10^{11}$ ions/cm^2" sample. Whereas the echo decay can be simulated with a single exponential, the fit of the saturation recovery kinetics necessitates the use of at least two exponentials of similar amplitude. From 10 K to room temperature the echo decay rate is constant. The rather long T_2 value of about 3 μs indicates that nuclear spin diffusion in the rather disperse ^{19}F spin reservoir is suppressed. The increase in T_2 at low temperatures indicates that there still is a contribution of electron spin dipolar processes which is quenched at low temperatures[14]. Increasing the concentration of paramagnetic centers by exposing the sample to a higher ion fluence ($2 \cdot 10^{12}$ ions/cm^2), we observed a shortening of T_2 by a factor 2, indicating that dipole-dipole interaction between paramagnetic centers is now dominating spin dephasing. The increase in spin lattice relaxation rate measured for the high fluence sample is even more pronounced, although a direct comparison of data was not made because of their multi-component time dependence.

B. ENDOR experiments

1. *Spectral analysis*

The rather long electronic relaxation rates allowed performing pulsed ENDOR experiments for a final identification of paramagnetic centers even with mw pulses as long as 500 ns. At an external field of 8.56 T, ENDOR transitions for ^6Li, ^7Li, and ^{19}F nuclei cover the range from about 20 to 450 MHz. Aiming at optimal frequency resolution not limited by the Fourier width of rf pulses, ENDOR experiments were performed at temperatures below 10 K. In this temperature range, rf pulses of 50 μs could be accommodated using Mims or Davies pulse

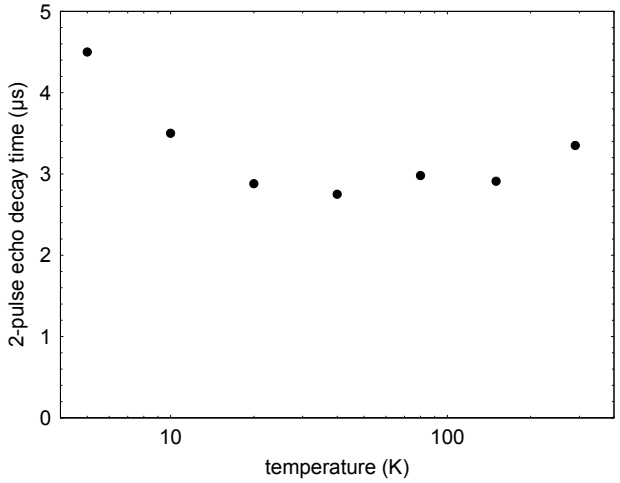

FIG. 2: Two pulse echo decay time as function of temperature. The echo sequence used was 400 - τ - 500 ns.

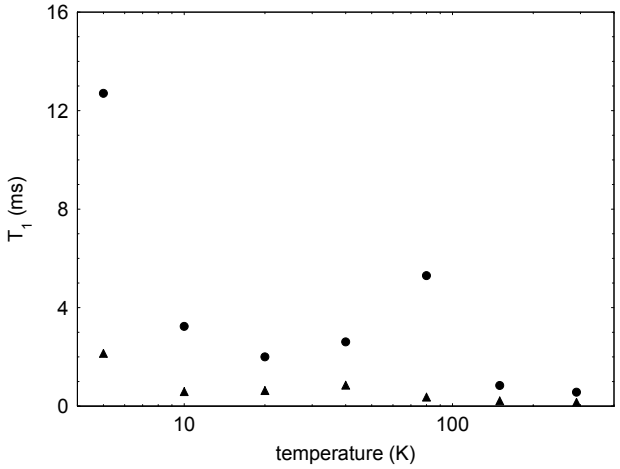

FIG. 3: Time constants of saturation recovery as function of temperature. Using the same echo sequence as in Fig. 2 with τ = 800 ns, the signal recovery after a first "inverting" pulse of 500 ns was recorded.

sequences by taking advantage of long T_1 values.

For the analysis of the observed ENDOR frequencies we use the following Hamiltonian for a single electron spins coupled with n nuclei

$$\mathcal{H} = g\mu_B \mathbf{BS} + \sum_{j=1}^{n} \{\gamma_N^j \mathbf{BI} + (a_{\rm iso}^j + A_{\rm zz}^j \frac{(3\cos^2\theta^j - 1)}{2})\mathbf{SI}\} \quad (1)$$

in which for each nucleus j $a_{\rm iso}^j$ is the isotropic hyperfine interaction, $A_{\rm zz}^j$ is the axial anisotropic hyperfine interaction, and θ^j represents the orientation with respect to the field, which is directed along a (100) direction.

In Fig. 4, the spectral range covering ^{19}F resonances is shown. On a slightly wavy baseline a strong multiline signal is detected around 343 MHz, when using a standard Mims sequence (see Fig. 4b). These lines are

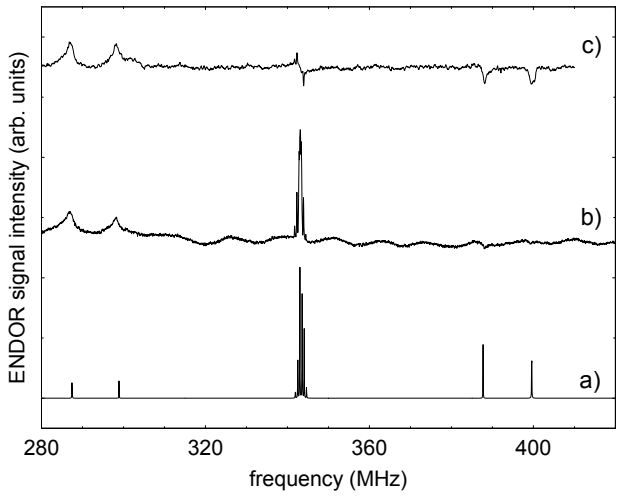

FIG. 4: 240 GHz pulsed ENDOR spectra (b, c) of Xe irradiated LiF in the ^{19}F spectral range measured at 8 K. Spectra were recorded using a Mims sequence consisting of three 450 ns mw pulses, the first pulses separated by 800 ns, the final pulse delayed by 60 μs. A simulated spectrum is shown in trace a). In b) the rf pulse of 50 μs duration was terminated just before the final mw pulse, in c) the rf pulse of equal length starts just after the stimulated echo.

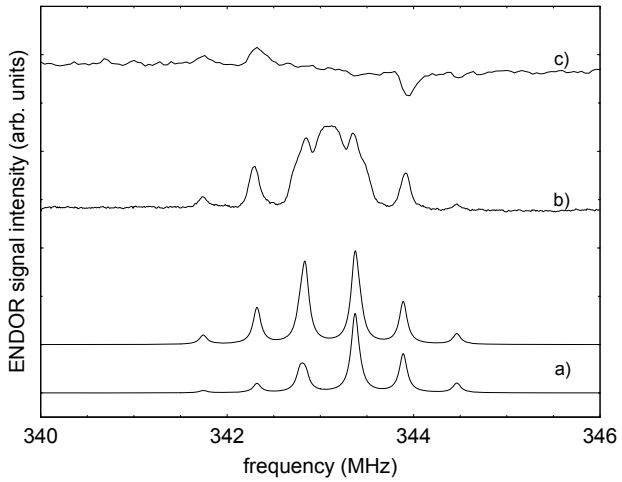

FIG. 5: 240 GHz pulsed ENDOR spectra (b, c) of Xe irradiated LiF close to the free ^{19}F frequency. In b) the rf pulse of 50 μs duration was terminated just before the final mw pulse, in c) the rf pulse of equal length starts just after the stimulated echo. Simulated spectra assuming a Lorentzian line shape (FWHM = 100 kHz) are shown for T = 80 K (a) upper trace) and T = 8 K (a) lower trace). Equal pulse lengths were used as described in Fig. 4.

centered at the ^{19}F Larmor frequency (B_0 = 8.56 T). In addition, a doublet separated by 15.6 MHz, its center shifted by 50.2 MHz to lower frequencies is also seen. As shown by the simulation using parameters compiled in Table 1, these resonances can be attributed to hfi with ^{19}F nuclei in the closest shell of anions located at regular positions around an anion vacancy (see Fig. 4a). The

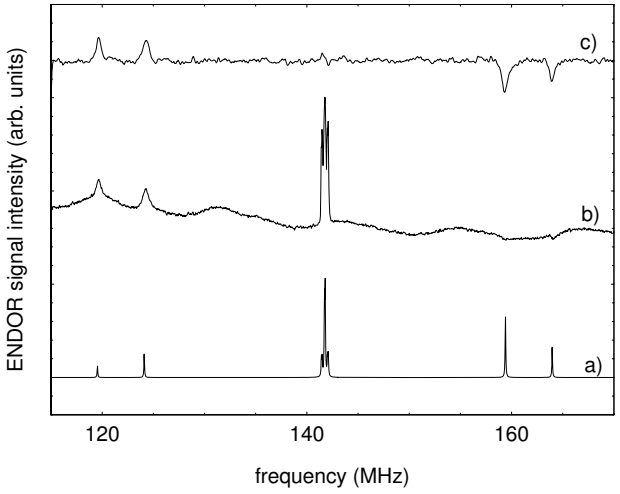

FIG. 6: 240 GHz pulsed ENDOR spectra (b, c) of Xe irradiated LiF in the ^7Li spectral range. A simulated spectrum is shown in trace a). Spectra were recorded using a Mims sequence consisting of three 450 ns mw pulses, the first pulses separated by 800 ns, the final pulse delayed by 60 μs. In b) the rf pulse of 50 μs duration was terminated just before the final mw pulse, in c) the rf pulse of equal length starts just after the stimulated echo.

effect of a time shifted rf pulse as documented in trace c) is discussed in section B2.

Using an expanded scale, a well resolved line multiplet is detected around the "free" ^{19}F frequency as shown in Fig. 5. Apart from the center, these signals can be assigned to fluorine spins in shells *IV* and *VI*. Spectral simulations were performed assuming Boltzmann-equilibrated conditions for 80 K and 8 K. The former set was used to facilitate the identification of lines. The apparent good match of experimental 8 K intensities with values predicted for the "high temperature case" is quite fortuitous, because the Boltzmann-equilibrated ENDOR line intensities calculated for 8 K are clearly different, showing the effect of depopulation of the upper m_S manifold.

For a further discussion the definition of nuclear positions around the anion vacancy given by Seidel[15] is used. An orientation of the external field perpendicular to the (001) plane of the crystal was assumed for spectral simulation. The relative orientation and site multiplicity of nuclei in shells *I* to *VI* is taken into account. Data are listed in Table *I*. Perfect agreement with the experimental spectrum confirms that the paramagnetic center formed by swift heavy ion bombardment is identical with the V_F center created by Xray and neutron irradiation, being investigated in detail many decades ago. We further note that apparently no noticeable disorder is seen, apart from some line broadening of the closest, strongly coupled fluorine nuclei in shell *II*. Although line positions were perfectly matched by the simulation, line intensities of the strongly coupled nuclei are at variance with prediction. The high frequency counterpart of shell *II* resonances was barely visible and found to be inverted in sign.

TABLE I: Distances and relative orientations of the principal axis of the axially symmetric dipole-dipole interaction tensor with respect to $B_0\|(100)$, assuming an undistorted local topology around the trapped electron at the F vacancy. Shell *I, II* values were determined by fitting the 240 GHz ENDOR spectra, other values are taken from Holton and Blum[3]. The distances are expressed in unit of the unit cell parameter a=0.403 nm.

shell	ion	uvw	d	mult	a_{iso} (MHz)	A_{zz}(MHz)
I	Li	100	0.5a	6	38.34	6.09
II	F	110	0.707a	12	104.4	31.2
III	Li	111	0.866a	8	0.5	1.36
IV	F	200	a	6	0.48	2.24
V	Li	210	1.118a	24	0.27	0.56
VI	F	211	1.225a	24	0.88	1.38

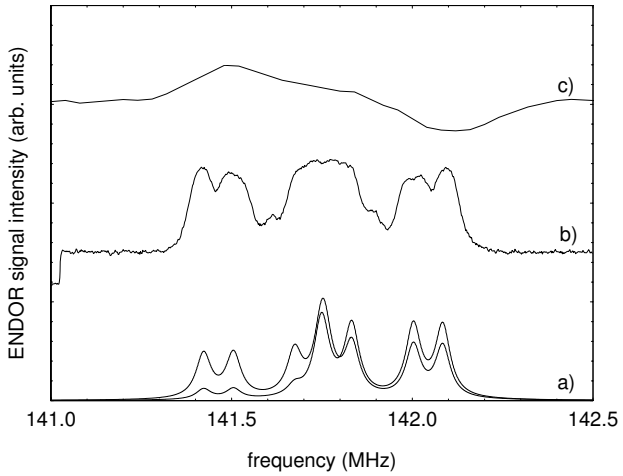

FIG. 7: 240 GHz pulsed ENDOR spectra (b, c) of Xe irradiated LiF close to the ^7Li frequency. Boltzmann-equilibrated spectra simulated for 80 K (line intensities nearly symmetrical with respect to the free ^7Li frequency) and 8 K are shown in traces a). Spectra were recorded using a Mims sequence consisting of three 450 ns mw pulses, the first pulses separated by 800 ns, the final pulse delayed by 60 μs. In b) the rf pulse of 50 μs duration was terminated just before the final mw pulse, in c) the rf pulse of equal length starts just after the stimulated echo. The weak spectrum c) was multiplied by a factor 10 to facilitate comparison.

In Fig. 6, the ENDOR spectral range covering ^7Li resonances is depicted. Again, strong resonances are found centered at the "free" ^7Li frequency, and also transitions assigned to strongly coupled nearest neighbor *Li* ions (shell *I*) are detected. Spectral simulation confirms this assignment. As in the case of ^{19}F resonances, the weakly coupled nuclei give rise to quite narrow ENDOR lines (50 kHz (FWHM)) (see Fig. 7, the lines of shell *I* being broadened to approximately 500 kHz. Second-order splittings as have been observed at X band can be

ruled out as reason for this line broadening because of the much higher Larmor frequency. It is also unlikely that unresolved quadrupole interaction causes line broadening for ^7Li spins (I = 3/2), because nearly the same effect is observed for the ^{19}F nuclei. We therefore suggest that the increased width of transitions assigned to shell I and II spins is caused by small distortions of the local topology around the vacancy leading to a distribution of hfi values.

In the ^7Li spectrum the deviation from expected line intensities is even more pronounced than for ^{19}F spins. The phase of the high frequency signals is definitely negative, i. e., the stimulated echo intensity increases for these lines, whereas the "normal" echo response in a Mims type experiment is a reduction of the absolute echo intensity.

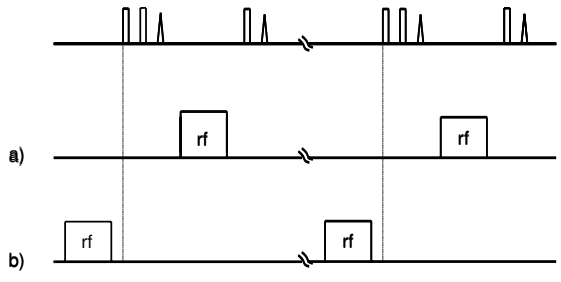

FIG. 8: Mw/rf pulse scheme used for ENDOR detection. The integrated echo intensity after the 3rd mw pulse is used as measure for the ENDOR effect. The rf pulse is applied either a) after the first two mw pulses ("standard" Mims set-up) or b) ending just before the start of the next mw pulse sequence.

2. Modelling ENDOR intensities

As was noted in the introduction, anomalous phase ENDOR signals have been detected quite frequently under conditions of high electron spin polarization. Theoretical concepts have been derived, allowing to use this phase information for determining the sign of the hfi constants[5,6]. These theoretical descriptions utilized the concept of dipolar order, being created by a sequence of mw pulses, and its dynamical interplay with electron spin relaxation. In subsequent publications [8,9] it was shown how to calculate the population differences of nuclear spin levels created by a repetitive combined mw/rf pulse sequence. Depending on the choice of relaxation parameters invoking electron spin lattice and cross relaxation rates, as well as nuclear spin lattice relaxation rates, the quasi equilibrium values of a four-level spin system can be derived as function of the pulse repetition time. As is shown in the following, a quite simple concept invoking only the deviation of the spectral density of spin packets at the selectively excited transitions from the unperturbed distribution function in thermal equilibrium ("hole and anti-hole burning"), can be used to describe qualitatively the negative phase effect observed under conditions of a repetitive mw/rf pulse sequence.

For a description of the observed "anti-phase" effect we consider a simple S = 1/2, I = 1/2 spin system as basic building block for the inhomogeneously broadened EPR transition. This broadening with spectral width much larger than the T_2-determined homogeneous line width is assumed to be caused by unresolved hfi. The mw pulse sequence is a standard Mims sequence consisting of three selective pulses of nominal $\pi/2$ length as shown in figure 8. Before application of the first two pulses of the pulse train, the spin system is assumed to be in thermal equilibrium. The corresponding density matrix can be described by $1 + S_z$. Nuclear polarization is neglected. After selective pulses exciting either pair of $m_I = +1/2$ or -1/2 sublevels, dipolar order S_zI_z of opposite sign is generated. The net dipolar order vanishes, however, because both sublevels are excited with equal probability if applying the sequence close to the center of the inhomogeneous line. Neglecting cross relaxation and spectral diffusion, spin lattice relaxation cannot lead to the generation of net dipolar order.

Pulse widths as well as pulse separation define the details of the resulting (nearly) periodic variations of $< S_z >$ as function of the offset from the applied mw frequency. This deviation of $< S_z >$ from the thermal equilibrium value is frequently called "population grating", although no change in the absolute number of spins contributing to the excited spin packets is induced after a non-repetitive pulse sequence. The pattern can be probed by a third pulse, its time domain response, the "stimulated echo" (SE) corresponding to the Fourier transform of the polarization grating. For a delay time T between second and third pulse large compared to electronic and nuclear dephasing times, only the diagonal elements of the density matrix have to be retained for a simulation of the SE. The resulting SE amplitude is depending on the amplitude of this $< S_z > - < S_z(eq) >$ pattern.

The effect of applying a repetitive SE pulse train can now be described by considering two limiting cases. First, the repetition rate is much less than any spin lattice relaxation rates. No difference to a single train analysis occurs. Second, the repetition rate is comparable to the electronic spin lattice relaxation rate. In this case there will be a dynamic equilibrium established by the competition of repetitive excitation and relaxation. The result will be depending on the frequency offset of spin packets. It should be noted, however, that spin packets with zero frequency offset can be treated quite easily, because in the limit of negligible relaxation during the 3-pulse train these spins are rotated by $3\pi/2$, leading to a vanishing expectation value of S_z immediately after the third pulse. In a repetitive pulse train the system will relax towards its thermal equilibrium value, but will be found at a higher spin temperature in general. Under typical experimental conditions, the spectral range of excited spins is much less than the inhomogeneous absorption width.

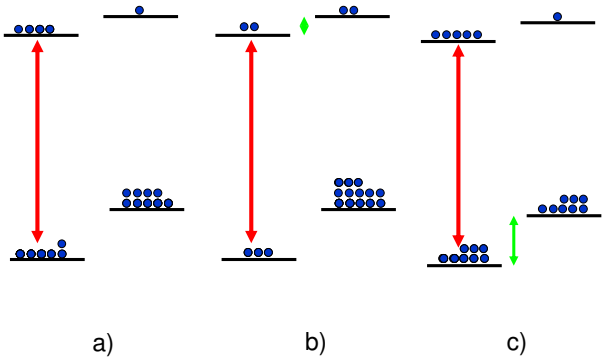

FIG. 9: (a) 'Average populations of the sublevels of a S=1/2, I=1/2 system with (pulsed) microwaves resonant with one of the hyperfine levels. (b) While also applying RF pulses resonant with the nuclear transition of the $m_s = 1/2$ manifold. (c) While applying RF pulses resonant with the nuclear transition of the $m_s = -1/2$ manifold. No cross relaxation is assumed.

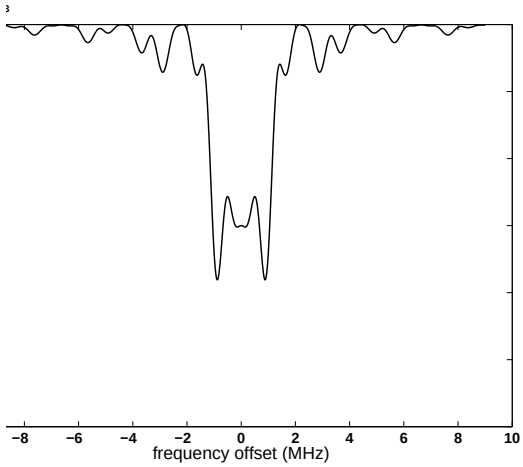

FIG. 10: Offset dependent polarization calculated for a Mims pulse sequence with $\tau_{\pi/2} = 450$ ns, first delay = 600 ns, T = 3 K, line width = 300 MHz (FWHM). Only the center part of the polarization pattern is shown.

In our case, a relative percentage of only about 10^{-3} of spins is excited, thus we can safely assume a constant bulk spin temperature of the sample. A decrease of the absolute SE amplitude is predicted and observed. This effect is frequently used to select an appropriate sequence repetition rate.

The situation becomes more interesting if resonant rf transitions within the nuclear spin manifold are considered. These transitions not only "destroy" the population difference grating but can also change the total number of spins, which are contributing to the number of spin packets probed by the mw pulses. Both effects will influence the SE amplitude. The former effect leads to a decrease of the absolute amplitude of the SE, its response setting the "phase" for the standard Mims ENDOR signal. In contrast, net population transfer can give rise to an increase or decrease of the SE amplitude. This is schematically illustrated in figure 9.

The contribution of the population transfer effect on the echo amplitude can be selectively observed by placing the rf pulse directly after the SE. If the pulse train repetition time is chosen much longer than the SE decay time, which is the standard procedure, no rf response occurs in the absence of population redistribution. For spin packets with zero frequency offset it is now easy to predict the effect of a resonant rf pulse applied after the mw pulse train. For these spin packets their upper and lower level populations are equal after the third pulse (see Fig. 10). This leads to a relative lower population of the mw driven ground state level and a higher population of the excited state with respect to the reference levels in the model four-level system. Net population transfer results, leading to anti-hole formation (ENDOR in the lower m_S manifold), or hole burning (ENDOR in the upper m_S manifold) with respect to the envelope of the inhomogeneous line. The ground state ENDOR transition therefore is predicted to increase the SE amplitude, leading to the anomalous phase of the ENDOR response, whereas the excited state ENDOR response is decreased, *i.e.*, the line is observed with the "standard" phase. In this simple picture, the absolute signal size is predicted to be equal. The amount of population transfer in a repetitive experiment will depend on the electronic Boltzmann factor and will be limited by nuclear spin relaxation and by spectral diffusion within the inhomogeneous EPR line. It should be noted that the same asymmetry arises if an elevated spin temperature of the selectively excited spin packets is considered. In the limit of selective spin packet heating both m_S levels are equally populated, leading to the same signature of hole and anti-hole formation.

Using this concept of hole and anti-hole burning by applying the rf pulse directly after the SE position, a simple recipe is obtained for the generation of anti-phase ENDOR signals of equal absolute size. This prediction does not depend on specific conditions for the various relaxation rates involved, as long as the nuclear spin relaxation rate is sufficiently small. This qualitative result is in agreement with the results of the numerical simulation of Morton et al. [9] using a Davies sequence.

The predicted effect of hole and anti-hole formation was tested by applying the rf pulse of 50 μs duration just after the SE in the repetitive three-pulse mw sequence, the sequence being repeated after 12 ms. In traces c) of Figs. 4, 5 the resulting ENDOR spectra covering the ^{19}F range are displayed. As expected, ENDOR transitions in both m_S manifolds are detected and found equal in amplitude within experimental error. The pulse train repetition time was chosen much larger than the SE decay time to ensure that the polarization grating had decayed at the beginning of the next pulse sequence. Under these conditions the ENDOR effect is predicted to originate

exclusively by population transfer, *sic.* hole and anti-hole formation, as is confirmed by anti-phase signals of equal amplitude.

In our case, we can safely assume a positive sign for the isotropic hfi constant. Accordingly, the high frequency ENDOR transition originates from the electronic ground state levels. It shows the "negative phase" signature in agreement with our qualitative analysis. The spectrum recorded in standard fashion apparently is a superposition of both effects, leading to a near cancellation of the high frequency signal intensity. It should be noted that according to the simulation these lines should be dominant in an equilibrated case at this temperature. Not taking into account the above described effects, this could lead to an erroneous sign assignment for this hfi constant.

A quite similar picture emerges when probing the ^7Li frequency range. The ENDOR spectra are displayed as traces c) in Figs. 6, 7. The "negative" ENDOR response is also observed for the high frequency transition, in accordance with the positive sign of the largest hfi constant. Transitions close to the "free" ^7Li frequencies are barely visible. This is in contrast to the ^{19}F case, for which "anti-phase" ENDOR signals are easily detected. The reason for this different behavior can be attributed to the smaller frequency shifts induced by ENDOR transitions of distant shell nuclei in the "upper" and "lower" m_S manifold caused by the relatively small ^7Li hfi. These frequency shifts in the order of 600 kHz are comparable to the microwave excitation width of about 1 MHz, efficient rf-driven hole and anti-hole formation therefor being impeded.

It should be noted that the relative intensity of the effects described are strongly enhanced if the temperature (kT) is of the order of magnitude or smaller than the frequency ($h\nu$). In figure 11 the effect of the population changes on the echo intensity in a pulsed EPR experiment is illustrated with and without resonant excitation of ENDOR transitions as a function of the $kT/h\nu$ ratio. The microwaves are sufficiently selective to not excite the other hyperfine component. The assumed population effects of the RF transition is assumed to equalize the population of the nuclear spin levels of the $m_s = +1/2$ and $m_s = -1/2$ manifolds respectively, as illustrated in figure 9.

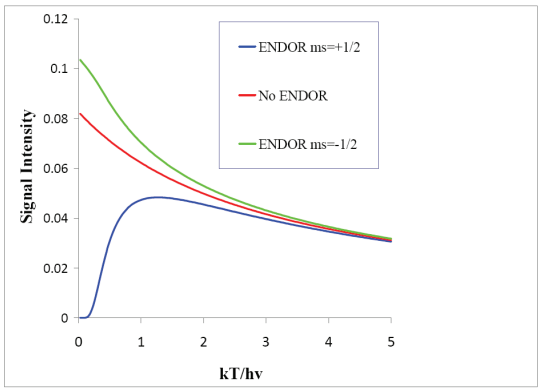

FIG. 11: The expected echo intensity of a pulsed EPR experiment if the shot repetition time is short with respect to T_1, while neglecting any nuclear and cross relaxation processes. Three cases are considered, without RF radiation, with RF radiation resonant with the ENDOR transition of the upper $m_s = +1/2$ manifold and with RF radiation resonant with the ENDOR transition of the lower $m_s = -1/2$ manifold.

IV. CONCLUSION

Performing pulsed ENDOR experiments at an electronic Larmor frequency of 240 GHz, the identity of paramagnetic centers generated by swift heavy ion irradiation of LiF crystals could be determined. In the cavity-free setup used, a sufficiently large microwave field at the sample could be generated by positioning the sample in front of a mirror at the end of a circular wave guide with 2 mm diameter. Well resolved ENDOR spectra resulting from hfi with ^7Li and ^{19}F nuclei in six different shells with the electron trapped at a vacancy at the regular anion site (F center) could be resolved. Taking advantage of the high electronic Zeeman energy, further line splitting or line broadening by second-order hfi in the highly degenerate nuclear spin system is effectively suppressed, thus leading to a relative spectral width of ENDOR transitions in the order of 10^{-4}. Even under conditions of high local energy loss as present under high ion impact energies, the local density of persistent F centers apparently is sufficiently low to prevent significant distortions of the cubic crystal structure. In the ENDOR spectra, there was no indication of different paramagnetic centers, which might have been hidden underneath the broad EPR absorption pattern.

When performing ENDOR under conditions of high electron spin polarization, a strong deviation from the ENDOR line intensities expected for a system in thermal equilibrium was noted. The effect was most pronounced when applying the rf pulse directly after the 3-pulse Mims-type mw sequence. Modelling the effect by neglecting coherences in the coupled spin system, a semi-quantitative picture emerges, allowing us to rationalize the relative amplitudes of the normal and anomalous phase signals. The observed "positive" and "negative" ENDOR response can be attributed to efficient hole and anti-hole formation in the inhomogeneously broadened EPR spectrum and can be used to determine the sign of the hfi coupling constants. As expected and confirmed by observation, hole and anti-hole burning is limited to ENDOR transitions with hfi larger than the spectral width of the mw excitation pulses.

V. ACKNOWLEDGMENTS

KPD is grateful for a visiting professor fellowship at the National High Magnetic Field Laboratory (NHMFL). C. w. EPR spectra were recorded with the help of A. Ozarowski (NHMFL). The National High Magnetic Field Laboratory is supported by the NSF Cooperative Agreement No. DMR- 0654118, by the State of Florida, and by the DOE.

* Electronic address: dinse@physik.fu-berlin.de

[1] H. Stork, K.-P. Dinse, F. Fujara, A. Hamburger, P. Jakes, R. Neumann, B. Schuster, K. Schwartz, and C. Trautmann, J. Phys. Condens. Matter **20**, 465215 (2008).
[2] K. Schwartz, A. E. Volkov, M. V. Sorokin, C. Trautmann, K.-O. Voss, R. Neumann, and M. Lang, Phys. Rev. B **78**, 024120 (2008).
[3] W. C. Holton and H. Blum, Phys. Rev. **125**, 89 (1962).
[4] R. Kaplan and J. Bray, Phys. Rev. **129**, 1919 (1963).
[5] M. T. Bennebroek and J. Schmidt, J. Magn. Reson. **128**, 199 (1997).
[6] B. Epel, A. Pöppl, P. Manikandan, S. Vega, and D. Goldfarb, J. Magn. Reson. **148**, 388 (2001).
[7] M. Bennati, N. Weiden, K.-P. Dinse, and R. Hedderich, J. Amer. Chem. Soc. **126**, 8378 (2004).
[8] S. Stoll, B. Epel, S. Vega, and D. Goldfarb, J. Chem. Phys. **127**, 164511 (2007).
[9] J. J. L. Morton, N. S. Lees, B. M. Hoffman, and S. Stoll, J. Magn. Reson. **191**, 315 (2008).
[10] S. Nellutla, G. Morley, M. Pati, N. Dalal, and J. van Tol, Phys. Rev. B **78**, 054426 (2008).
[11] J. van Tol, L. C. Brunel, and P. Wyder, Bull. Am. Phys. Soc. **44**, 1130 (1999).
[12] J. van Tol, K.-P. Dinse, H. Kungl, and M. Hoffmann, Appl. Magn. Reson. **36**, 297 (2009).
[13] J. F. Ziegler, J. Appl. Phys./Rev. Appl. Phys. **85**, 1249 (1999).
[14] S. Takahashi, R. Hanson, J. van Tol, M. S. Sherwin, and D. Awschalom, Phys. Rev. Lett. **101**, 047601 (2008).
[15] H. Seidel, Z. Physik **165**, 218 (1961).